



CHALMERS
UNIVERSITY OF TECHNOLOGY

Resolving the orbital character of low-energy excitations in Mott insulator with intermediate spin-orbit coupling

Downloaded from: <https://research.chalmers.se>, 2025-07-01 19:49 UTC

Citation for the original published paper (version of record):

von Arx, K., Rothenbühler, P., Wang, Q. et al (2025). Resolving the orbital character of low-energy excitations in Mott insulator with intermediate spin-orbit coupling. *Communications Physics*, 8(1). <http://dx.doi.org/10.1038/s42005-025-02104-2>

N.B. When citing this work, cite the original published paper.

<https://doi.org/10.1038/s42005-025-02104-2>

Resolving the orbital character of low-energy excitations in Mott insulator with intermediate spin-orbit coupling

Check for updates

Karin von Arx ^{1,2}, Pascal Rothenbühler², Qisi Wang ^{2,3}, Leonardo Martinelli², Jaewon Choi ⁴, Mirian Garcia-Fernandez ⁴, Stefano Agrestini ⁴, Ke-Jin Zhou ⁴, Antonio Vecchione ^{5,6}, Rosalba Fittipaldi ^{5,6}, Yasmine Sassa ^{1,7}, Mario Cuoco ^{5,6}, Filomena Forte ^{5,6} ✉ & Johan Chang ²

Multi-band Mott insulators with moderate spin-orbit and Hund's coupling are key reference points for theoretical concept developments of correlated electron systems. The ruthenate Mott insulator Ca_2RuO_4 has therefore been intensively studied by spectroscopic probes. However, it has been challenging to resolve the fundamental excitations emerging from the hierarchy of electronic energy scales. Here we apply high resolution resonant inelastic x-ray scattering to probe deeper into the low-energy electronic excitations found in Ca_2RuO_4 . In this fashion, we probe a series of spin-orbital excitations. By taking advantage of enhanced energy resolution, we probe a 40 meV mode through the oxygen *K*-edge. The polarization dependence of this low-energy excitations exposes a distinct orbital nature, originating from the interplay of spin-orbit coupling and octahedral rotations. Additionally, we discuss the role of magnetic correlations to describe the occurrence of excitations with amplitudes which are multiple of a given energy. Such direct determination of relevant electronic energy scales sharpens the target for theory developments of Mott insulators' orbital degree of freedom.

Materials with moderate to strong spin-orbit coupling (SOC) have long been the center of intense research¹. In some material classes - such as the iridates—SOC is a key driver of multi band Mott physics². In metals, SOC plays a role in problems linked to topology^{3,4}. A third pillar is the combination of SOC and magnetism^{5,6}. In such systems, spin and orbital excitations can no longer be treated separately. This setting offers a ground for new types of collective excitations but also adds further layers of complexity to both theory and experimental efforts. On the experimental side, resonant inelastic x-ray scattering (RIXS) offers a unique possibility by being sensitive to both spin and orbital excitations⁷. However, only few systems with magnetic excitations also have a sizeable SOC. Most often, these energy scales are inaccessible to RIXS due to modest energy resolution. Recently, advances in soft RIXS methodology has greatly improved the energy resolution⁸. This yields new opportunities to tackle the problem of spin-orbit coupled magnetic ground states.

For example, in the archetypal multi-band Mott insulator Ca_2RuO_4 ^{9–13}, many questions related to low-energy scales are still open. Previous RIXS studies^{14–16} have revealed a series of excitations emerging from the interplay of Coulomb interaction U , Hund's coupling J_H , crystal-field splitting Δ and

SOC λ . It has been shown that SOC is a crucial element to explain the nature of these excitations and the activation in the RIXS process. However, theoretical modelling of the RIXS spectra only allows for an estimation of the relative strength of crystal-field and SOC, but the value of SOC is imprinted in the fine structure of an excitation sector. This fine structure, as well as a spin excitation predicted by the model around 40 meV, could previously not be resolved due to limited energy resolution.

Here we present a high-resolution (12.5 meV half-width half-maximum) oxygen *K*-edge RIXS experiment on Ca_2RuO_4 . This approach allows for a deeper insight into the low-energy structure of this SOC-driven multiband Mott insulator. In particular, the pristine resolution permits to resolve a 40 meV mode and to reveal the dispersive nature of the 80 meV mode. Our theoretical modelling suggests a complex spin-orbital origin of these modes. The orbital character of these excitation modes corresponding to longitudinal and transverse variation of the orbital angular momentum is thus inferred. Additionally, excitations at 160, 350, and 750 meV are observed. The fine structure (energy level splitting) of the 350 meV excitation revealed further insight into the SOC. Thus, the improvement in energy resolution allows for a detailed observation of the excitation spectrum and

¹Department of Physics, Chalmers University of Technology, Göteborg, Sweden. ²Physik-Institut, Universität Zürich, Zürich, Switzerland. ³Department of Physics, The Chinese University of Hong Kong, Shatin, Hong Kong, China. ⁴Diamond Light Source, Harwell Campus, Didcot, Oxfordshire, UK. ⁵CNR-SPIN, Fisciano, Salerno, Italy. ⁶Dipartimento di Fisica "E.R. Caianiello", Università di Salerno, Fisciano, Salerno, Italy. ⁷ Department of Applied Physics, KTH Royal Institute of Technology, SE-106 91 Stockholm, Sweden. ✉ e-mail: filomena.forte@spin.cnr.it

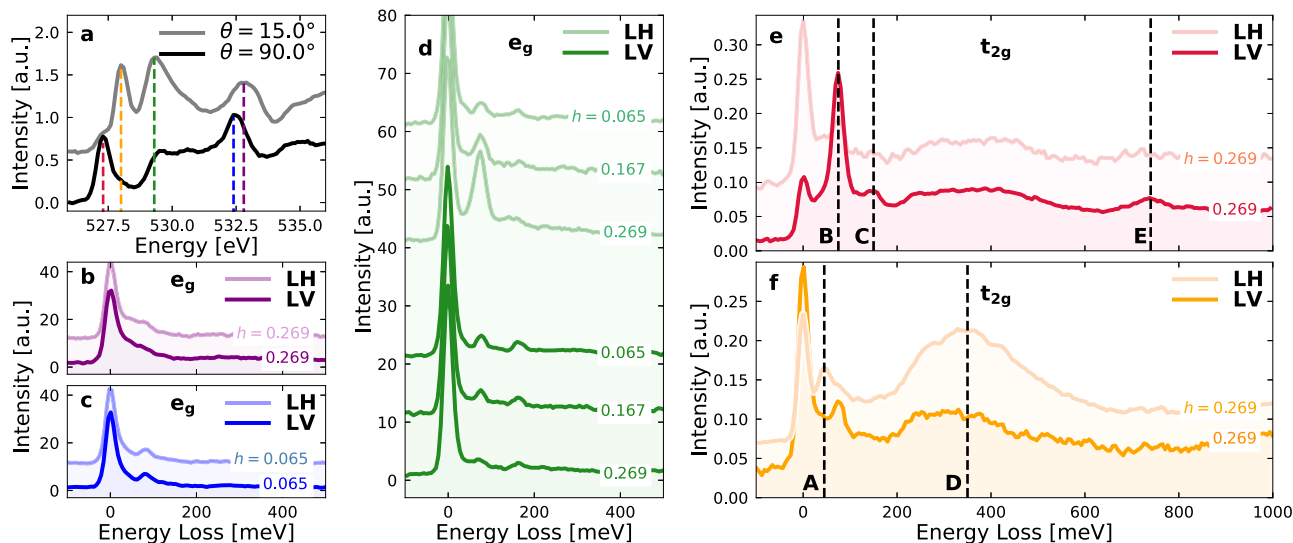


Fig. 1 | X-ray absorption spectroscopy (XAS) and resonant inelastic x-ray scattering (RIXS) on Ca_2RuO_4 . **a** X-ray absorption spectra at the oxygen K -edge recorded with linear horizontal (LH) polarized light and incidence angle as indicated (see Supplementary note 1). Dashed colored lines indicate the absorption resonances used to collect RIXS spectra in (b–f). **b–d** RIXS spectra (intensity versus energy loss) obtained

on the e_g resonances for LH and linear vertical (LV) light polarizations and momentum $q = (h, 0)$ where h is indicated for each spectra. **e, f** Spectra recorded on the t_{2g} resonances. Vertical dashed lines in (e) and (f) indicate the observed excitations—labeled A, B, C, D, and E. The color code in (b–f) matches the resonance identification (vertical dashed lines) in (a). Discussion of statistical errors is found in the Supplementary note 2.

the precise extraction of the SOC fine structure, which is essential for understanding the complex and rich properties of Ca_2RuO_4 .

Results

Figure 1 a displays oxygen K -edge x-ray absorption spectra recorded with linear horizontal polarized light for different angles θ between sample surface and incident light as indicated. The two pre-edges originating from the hybridisation of the oxygen orbitals with the ruthenium t_{2g} states split due to the different crystal field environment around the planar and apical oxygen sites. These t_{2g} resonances are followed by broader e_g resonances. RIXS spectra are collected at both the t_{2g} and e_g resonances—see Fig. 1b–f using both linear vertical (LV) and horizontal (LH) light polarizations. In total, five (low-energy) excitations, labeled A, B, C, D, and E, are found in the t_{2g} spectra. The e_g and t_{2g} spectra both display excitations at 80 meV and 160 meV (B,C). We stress that excitations B, D, and E at 80, 350, and 750 meV, have been reported in previous RIXS studies^{14–16}. Yet, with increased energy resolution we reveal additional information about these excitations. Excitation A and C are to the best of our knowledge reported here for the first time. The energy scale of the A excitation matches with both transverse and longitudinal magnetic modes reported by neutron scattering in Ca_2RuO_4 ¹⁷. We also stress that in oxides with similar perovskite structures, a bond-buckling mode is reported with this energy scale¹⁸. In this context of phonon and magnon modes, it is worth noticing that excitation B is found at twice the energy of excitation A, excitation C at twice the energy of B and these three excitations are observed at the same absorption resonances and light polarizations. This strongly suggests that these three excitations are connected.

The A and B excitations—after subtracting the elastic scattering profile—are shown in Fig. 2. The B excitation is most pronounced in the LV channel at the apical oxygen site where it manifests strongly for all h measured along $(h, 0)$ (see Fig. 2a, c). The A excitation is most clearly observed with LH polarization at the planar oxygen site (see Fig. 2b, d) for large momentum transfers. Interestingly, the intensity amplitude of this excitation decays as the zone center is approached. By contrast, the B excitation shows the opposite trend under these experimental conditions, being strongest at the zone center. Momentum dependence analysis of the A and B excitations reveal that B is dispersing clearly to lower energies upon increasing momentum. With our applied energy resolution, we cannot resolve any significant dispersion of the A excitation.

Next, the results of the D excitation are discussed. This excitation block is only observed at the t_{2g} -resonances—see Fig. 1. The absence of this D-block on the e_g resonances reinforce the interpretation of an inter- t_{2g} excitation. Previous experimental data identified two excitations¹⁴ in this D-block. With the improved energy resolution ($29 \rightarrow 12.5$ meV half-width half-maximum) and possible also sample quality, it is now clear that this block has at least three components, as can be seen for different momenta in Fig. 3. However, the broadly overlapping components (on an irregular background) make fitting models inconclusive.

The theoretical model introduced earlier¹⁴ predicts a splitting of the energy level around 350 meV in four components due to SOC. The assignment of the RIXS features is well understood in the simplified atomic picture, where all the low-energy states are written as linear combinations of the $|L_z, S_z\rangle$ vectors, expressed in terms of the z projections of the $S = 1$ and $L = 1$ moments within the t_{2g}^4 Ru manifold. In this framework, the lowest excitation contributing to the 350 meV structure is ascribed to the atomic transition between the ground state and the excited state $|D_1\rangle = \alpha|1, -1\rangle - \beta|-1, 1\rangle$, with specific expression of the α and β coefficient depending on the tetragonal crystal field splitting Δ and the SOC λ ¹⁴.

For O K -edge RIXS, the local scattering process is spin-conserving because of the absence of SOC in the core hole intermediate state. It turns out that the transitions induced at the Ru site between the dominant part of the spin-orbital configuration that contributes to the magnetic ground state (being mostly due to the $|0, 0\rangle$ state) and the D_1 state are not allowed, since they correspond to $\Delta S_z = \pm 1$ and $\Delta L_z = \mp 1$ ¹⁴.

The only non-vanishing dipole allowed atomic transitions to the D_1 state come from initial configurations $|1, -1\rangle$ and $|-1, 1\rangle$, which are spin-orbit activated in the atomic ground state. Such configurations have a negligible weight in the ground state, due to the modest SOC, and thus contribute with a negligible amplitude to the cross-section.

Thus, the three features seen in the RIXS spectrum around 300 meV can be associated to the higher energy levels D_{2-4} . From the data, the excitation energies of the A and middle D_3 modes (indicated by black dashed lines in Fig. 3) can be extracted to 37 and 340 meV, respectively. Within the theoretical model, these energies are set by the crystal field Δ and SOC λ . Using the excitation energies, we derive approximately $\Delta \approx 250$ and $\lambda \approx 85$ meV.

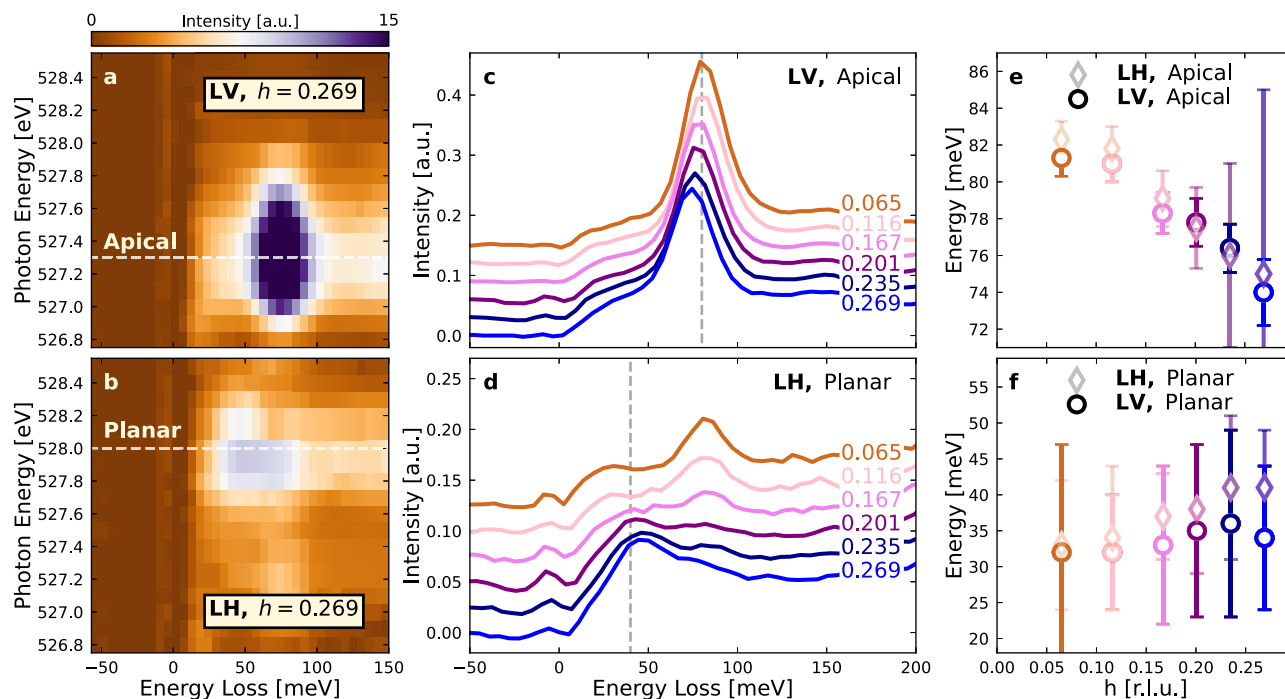


Fig. 2 | Low-energy resonant inelastic x-ray scattering (RIXS) spectra recorded on Ca₂RuO₄. **a, b** RIXS spectra as a function of incident photon-energy (vertical axis) for linear vertical and horizontal light and momentum as indicated. Horizontal dashed lines mark respectively the planar and apical oxygen pre-edges. Intensity is displayed using a linear false color scale. **c, d** RIXS spectra versus momentum as indicated. Vertical dashed lines are guides to the eye for the A and B excitations. To

highlight the low-energy excitations, elastic scattering is subtracted in (a–d). Spectra before subtraction are shown in Supplementary Fig. 3 in the Supplementary note 3. The dispersions—obtained from fits shown in Supplementary Fig. 4—of the A and B excitations are shown in (e, f). Error bars indicate 3σ standard deviations. From (c, e), a significant dispersion of the B excitation is resolved. Within error bars no dispersion is derived for the A excitation.

Discussion

Starting from the low energy side of the excitation spectrum, this work presents the detection of the 40 meV excitation mode by RIXS. Previously, an inelastic neutron scattering study reported a dispersive Higgs mode with a similar energy scale at the zone center¹⁷. Additionally, a theoretical framework from recent RIXS studies^{14,19} predicted a magnetic mode at approximately 40 meV, which should be observable through the RIXS cross-section. However, this energy range was previously not accessible in experiments due to limited instrumental energy resolution. With the high energy resolution applied in this study, it is now possible to confirm and resolve this mode by RIXS. Moreover, the RIXS cross-section is sensitive to angular-momentum through incident light polarization and incident light angle.

Before discussing this in greater detail, we stress that the 40, 80, and 160 meV excitations appear with doubling energy scales—potentially suggesting a connected origin. A phononic nature of especially the 80 meV excitation is, however, possible and should be considered. Many oxide systems (for example cuprates^{20,21} and titanates²²) have optical phonon branches in the energy range of 60–90 meV. In Ca₂RuO₄, Raman spectroscopy observes the high energy phonon just below 80 meV²³. We point out that in the same Raman measurements, a structure at around 80 meV has also been measured, and attributed to a magnetic excitation according to its temperature dependence.

Here, on the other hand, the excitation exceeds 80 meV at the zone center, as seen from the extracted dispersion (Fig. 2e). An observation is that the dispersion is significantly larger than expected for an optical phonon. Finally, observation of a phonon in the RIXS spectra requires the existence of a finite electron-phonon coupling. The extraction of electron-phonon coupling from intensity ratios between primary and higher harmonics phonon excitations is still being debated^{24,25}. Irrespectively of model choice, our observations are not suggesting a strong electron-phonon coupling. Phonons are certainly present in Ca₂RuO₄. Yet, we interpret the RIXS spectra through an electronic model, as described below.

Let us then consider the spin and orbital character of the low energy excitations (below 200 meV) and their relation to the different polarization channels at the planar and apical oxygen sites. An interesting question to consider is whether such low energy excitations are detectable by RIXS at the K-edge at both the apical and planar oxygen resonances. To provide answers, we consider a microscopic model which, at the Ru sites, includes the Coulomb interactions described via the intra-orbital repulsion U and Hund’s exchange J_H , and SOC term parametrized by λ . The local splitting between the d_{xy} and d_{xz}, d_{yz} orbitals due to the octahedral crystal field is also included, and expressed in terms of the amplitude Δ . Symmetry allowed hybridization processes between Ru and planar/apical O orbitals is also imposed. The full microscopic model is presented in the Supplementary note 4. For the present analysis, we adopt material specific values such as $\lambda = 0.075$ eV, $U = 2.2$ eV, $J_H = 0.4$ eV and $\Delta = 0.3$ eV¹⁹. Similar values for Δ , U , and J_H have been used for calculations of electronic spectra in Ca₂RuO₄, and the ratio $g = \Delta/(2\lambda)$ is typically considered to lie in the range $\sim [1.5, 2]$ for modelling the spin excitations observed by neutron scattering^{17,26}. The model Hamiltonian is then adapted to a finite size cluster consisting of two apical oxygens (O_a) and one central planar (O_p) oxygen site, thus having the following structure O_a –Ru– O_p –Ru– O_a . This cluster structure allows us to simultaneously access the RIXS cross section at the planar and apical oxygen. The simulated RIXS intensity I_{RIXS} at the planar and apical oxygen atoms is then calculated within the Fast Collision approximation, as detailed in the Supplementary note 6. In Fig. 4 the calculated RIXS responses show that the features at about 40 meV (A-mode), 80 meV (B-mode) and, with smaller relative intensity, at about 120 and 160 meV (C-mode) can be observed both at the apical and planar sites. This outcome can account for the fact that in LV apical and LH planar spectra (Fig. 2) one can observe non-vanishing peaks around 40, 80, 120, and 160 meV. Concerning the polarization dependence, we point out that our calculation cannot capture the different intensity in the LH and LV polarization shown by the A and B modes. This is because, due to the large space of

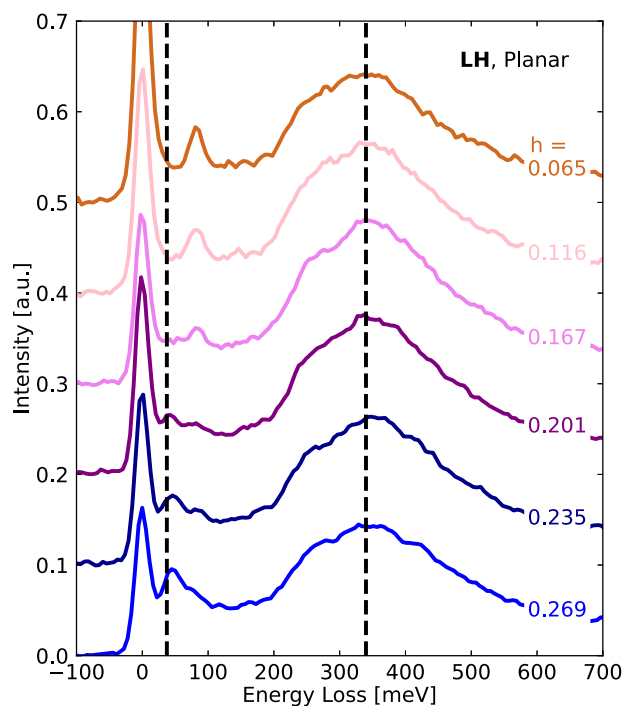


Fig. 3 | Resolved energy level splitting due to spin-orbit coupling. Spectra focusing on the excitation around 350 meV, recorded at different in-plane momenta as indicated. Black vertical dashed lines represent the excitation values extracted from the data used to calculate crystal field and spin-orbit coupling.

quantum states, the simulation has been done in an effective way by selecting a minimum physically relevant set of oxygens orbitals at the apical site. Another argument to be mentioned is that, as also mentioned above, there might be a spin-phonon contribution in the LV apical channel which enhances the spectral weight, and such contribution is not included in the analysis.

Concerning the character of these excitations, it is useful to consider the dynamical spin and orbital response described by the structure factors $S(q, \omega)$ and $L(q, \omega)$, related to the localized spin and orbital angular momenta of the d -electrons at the Ru site. For our purposes, the analysis of the orbital dynamics is particularly relevant because the weight of the RIXS spectra exhibits a sizable dependence on the light polarization, incidence angle and on the chosen (planar or apical) oxygen resonance. First, we recall that the magnetic ground-state has anisotropic antiferromagnetic correlations among the Ru spins with moments mostly lying within the ab plane^{19,27,28}. The lowest energy manifold is marked by excitations at about 40 meV and 80 meV. The modes at 80 meV are due to composite magnetic excitations, with dominant transverse character with multiple spin modes, which are allowed among the lowest-energy manifold, due to the SOC at the Ru site (see Supplementary Fig. 5 in the Supplementary note 5). This is consistent with the analysis done for a smaller cluster size¹⁹.

On the other hand, the low-energy peaks at about 40 meV arise from transverse spin modes, i.e., resulting from the S^\perp correlation function (symbol \perp refers to the component in the plane orthogonal to the magnetic easy axis), with a mark of having a non-trivial phase factor for the spin modes at nearest neighbor Ru sites as shown in Supplementary Fig. 5. Such non-local (inter-site) spin excitations can be accessible at both the planar and apical oxygens due to the rotation of the octahedra that provides a sublattice structure for the Ru network.

Due to the limited size of the cluster under examination, it is not possible to directly calculate the dispersion of the 40 and 80 meV features.

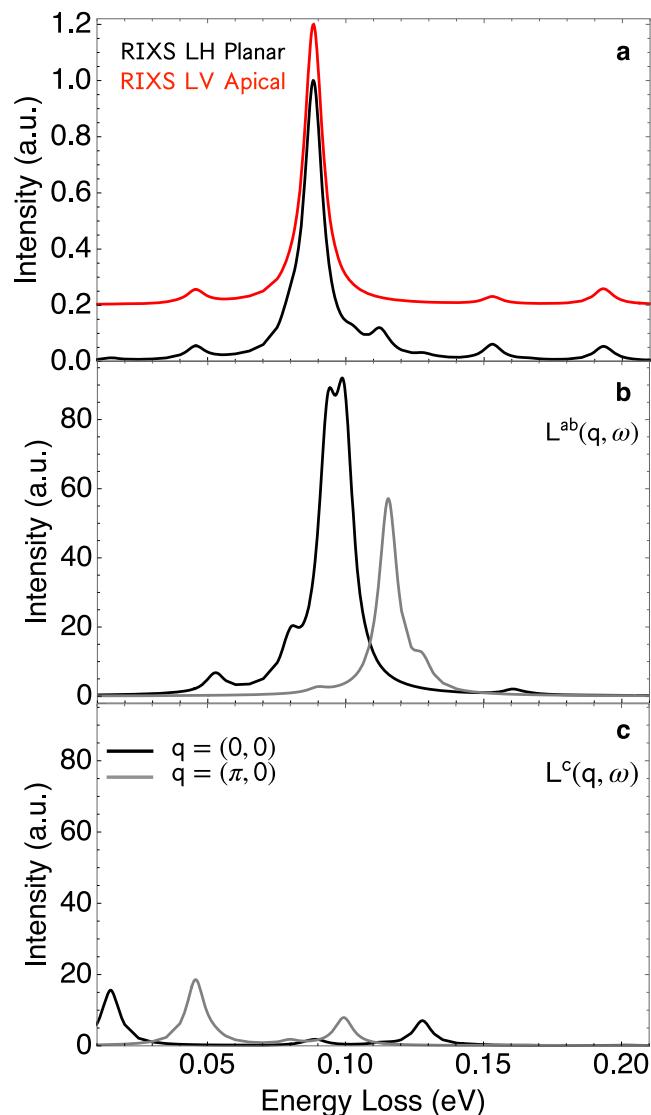


Fig. 4 | Theoretical resonant inelastic x-ray scattering (RIXS) and dynamical orbital structure factor spectra. **a** Calculated RIXS spectra at $q = (0, 0)$, for the finite size cluster as described in the discussion section. The black line represents the spectrum obtained for linear horizontal (LH) planar resonance, while the red line corresponds to the spectrum for linear vertical (LV) apical resonance. The spectra were broadened with a 4 meV full width at half maximum (FWHM) Gaussian. **b** Dynamical orbital angular momentum structure factor $L^{ab}(q, \omega)$, related to the component of the orbital angular momentum in the (a, b) plane (plane of the magnetic easy axis), calculated at $q = (0, 0)$ (black line) and $q = (\pi, 0)$ (gray line). **c** The dynamical orbital structure factor $L^c(q, \omega)$ related to the component of the orbital angular momentum along c direction.

Despite this, some considerations can be made about the theoretical estimates of the bandwidth. Local spin/orbital excitations may acquire a dispersion through processes involving virtual charge excitations on neighboring ruthenium sites. In previous works^{14,17} the bandwidth for single spin-flip processes has been estimated around 20 meV. We argue that a similar amplitude can also be associated to the single- and two-magnon like excitations.

Finally, we point out that the whole manifold of modes below 200 meV appear with energies that are multiples of the lowest energy mode at 40 meV. Hence, we argue that they may share a common nature which has a spin content related to multiple magnon excitations which can occur in the

system. This statement is corroborated by the outcomes of the analysis as shown in Fig. 4b, c and in Supplementary Fig. 5.

After having discussed the spin character of the excitations at 40 meV and 80 meV, we consider in more details the orbital nature of these modes. Due to the fact that the energy scales of the SOC and the crystal field are comparable, the lowest-energy excitations are marked by entangled spin-orbital configurations that involve both the spin S and orbital L angular momentum of the d -electrons at the Ru site. In this regime of crystalline environment, the orbital and spin excitations are thus expected to be anisotropic. One can then ask whether such orbital modes can be excited in RIXS at the O K -edge in the examined range of energy, and which dependence occurs on the direction of the excited orbital moments.

This discussion on the orbital character of the low-energy modes will help to account for the polarization and incident angle dependence of the RIXS spectra at the planar and apical resonance. To this end, in Fig. 4b, c we report the dynamical orbital response $L(q, \omega)$, resulting from the orbital angular momentum correlations at different time, for the two Ru sites on the examined cluster. We consider the possibility of having longitudinal orbital excitations associated with in-plane orbital correlations (L_{ab}) and transverse orbital modes resulting from out-of-plane orbital correlations (L_c). This separation is related to the anisotropy of the ground state, having orbital moments lying predominantly in the ab plane. Additionally, we analyze both the correlators with equal [opposite] phase at the Ru sites, corresponding to the $q = (0, 0)[\pi, 0]$ modes in the dynamical response, respectively. As shown in Figs. 4b, c we find that the in-plane orbital excitations are mainly accessible at energies around 80 meV. Instead, the out-of-plane orbital modes occur at lower energies, namely in the range of 40 meV and below it.

Taking into account these results, we can qualitatively discuss the polarization and oxygen resonance dependence of the RIXS spectra. The first remark we make regards the energy distribution of the orbital excitations. We find that the peaks at 80 meV have longitudinal character, namely the excitations at those energies can be achieved by inducing a variation of the orbital angular momentum in the ab plane. By contrast, the low-energy structure around 40 meV is mostly due to excitations that are achieved by orbital modes with out-of-plane orbital angular momentum, having transverse character.

It is worth pointing out that these excitations correspond to variation of the orbital angular momentum rather than of the occupation of the t_{2g} orbitals. This is why they occur at lower energy as compared to the crystal-field derived multiplet structure at about 300 meV. The orbital nature of the excited states below 100 meV can be put in connection with the polarization dependence of the RIXS spectra. Although not immediate, we observe that the photon electric field polarization aligned in the ab plane (or along c -axis) is mainly related to the variation of the orbital polarization at the Ru site in-plane (or along the c -axis). To get a deeper insight about this connection, one has to consider the d - p hybridized configurations of the type d^1-p^2/d^2-p^1 that are relevant for the transitions at the oxygen K -edge. In particular, the d^2-p^1 states that enter in the absorption process at the oxygen K -edges can filter configurations with different projections of the orbital angular momentum, depending on the occupation of the orbitals in the t_{2g} manifold. For instance, if the single occupied configuration lies in the xy orbital, then the L_x and L_y components of the orbital angular momentum will be more relevant. The behavior of the dynamical orbital response can thus be used to account for the observation of RIXS spectra in LV polarization at the apical oxygen, that exhibits a dominant spectral weight at high energies around 80 meV. This is a direct consequence of the fact that the p_y orbitals of apical oxygens are mainly accessible in LV polarization, and that the corresponding hybridized states are related to variation of the in-plane component of the orbital moments at the Ru site.

On the other hand, for the planar oxygen, the orbitals involved in the hybridization processes can be linked to both in-plane and out-of-plane variation of the orbital polarization at the Ru site. This implies that the RIXS spectra have peaks both around 40 and 80 meV. We speculate that the transfer

of spectral weight from the 80 meV to the 40 meV feature, that is obtained at the planar resonance by increasing the transferred momentum, can be related to the variation of the photon polarization direction. At higher momentum, the photon polarization aligns more in the out-of-plane direction and thus, according to the previous arguments, there is a transfer of spectral weight to low energy. Hence, one may conclude that the in-plane (out-of-plane) variation of the orbital polarization at the Ru site is more relevant for the vertical (horizontal) polarization of the photon electric field, respectively.

Conclusions

In summary, this work presents an ultra-high-resolution RIXS study of the multiband Mott insulator Ca_2RuO_4 , resolving the low-energy excitation spectrum and giving direct insight into spin-orbit coupled excitation modes. The measured excitation spectrum and its theoretical modelling explain how the lowest excitations at 40 and 80 meV are highly non-trivial with a strong spin-orbital character and accessible via RIXS at different light polarizations and absorption resonances through moderate SOC. Thus, we track the magnetic excitation spectrum and at the same time infer information about the orbital character. This adds crucial information to the magnetic fine structure of this Mott insulator. The rich low-energy excitation structure of this compound is also a fingerprint of its delicate interplay between different energy scales, demonstrating the significant role of SOC. We stress that the evidence for the presence of spin excitations, and in particular the feature at 40 meV, is based on (i) a deviation in the width of the peak from the instrumental resolution, (ii) the fact that magnetic excitations are accessible at the O K -edge of transition metals, as theoretically demonstrated to result from atomic SOC and inversion symmetry breaking at the O site²⁹, and (iii) the observation of a magnetic excitation in that energy range from neutron scattering¹⁷. While phononic modes can occur at similar energies, disentangling phononic and magnetic excitations in RIXS remains a significant challenge, beyond the scope of the current investigation, which will be addressed in future work.

Methods

High quality single crystals of Ca_2RuO_4 were grown by the floating zone techniques^{30,31}. Crystals were aligned ex-situ with x-ray LAUE and cleaved in-situ using a standard top-post technique. Thermal contact to the cryo-manipulator was achieved using the EPO-TEK E4110 silver epoxy cured overnight at 70^o₂₆. Oxygen K -edge x-ray absorption and RIXS were carried out at the I21 beamline at the DIAMOND synchrotron⁸. All data was recorded at a sample temperature of 15 K. Elastic scattering from a carbon tape yields an energy resolution of 12.5 meV half-width half-maximum (corresponding to standard deviation $\sigma = 10.6$ meV and FWHM = 25 meV), more than two times better than previous RIXS studies of Ca_2RuO_4 ¹⁴. As Ca_2RuO_4 is a quasi two-dimensional material, we project momentum transfer into $Q = (h, k)$. Furthermore, as RIXS spectra were collected in-plane along the Ru-O bond direction only, we use tetragonal notation to indicate momentum space despite orthorhombic crystal structure. This choice also facilitates comparison to existing literature on the topic. All RIXS spectra were normalized to the integrated spectral weight of the dd excitations.

Data availability

The data that support the findings of this study are available at Zenodo <https://doi.org/10.5281/zenodo.11395839>.

Received: 23 February 2024; Accepted: 17 April 2025;

Published online: 22 May 2025

References

1. Witczak-Krempa, W., Chen, G., Kim, Y. B. & Balents, L. Correlated quantum phenomena in the strong spin-orbit regime. *Annu. Rev. Condens. Matter Phys.* **5**, 57–82 (2014).
2. Kim, B. J. et al. Novel Jeff = 1/2 mott state induced by relativistic spin-orbit coupling in Sr_2IrO_4 . *Phys. Rev. Lett.* **101**, 076402 (2008).

3. Pesin, D. & Balents, L. Mott physics and band topology in materials with strong spin–orbit interaction. *Nat. Phys.* **6**, 376–381 (2010).
4. Bernevig, B. A., Hughes, T. L. & Zhang, S.-C. Quantum spin hall effect and topological phase transition in HgTe quantum wells. *Science* **314**, 1757–1761 (2006).
5. Chen, G. & Balents, L. Spin-orbit effects in $\text{Na}_4\text{Ir}_3\text{O}_8$: a hyper-kagome lattice antiferromagnet. *Phys. Rev. B* **78**, 094403 (2008).
6. Kunkemöller, S. et al. Highly anisotropic magnon dispersion in Ca_2RuO_4 : evidence for strong spin orbit coupling. *Phys. Rev. Lett.* **115**, 247201 (2015).
7. Ament, L. J. P., van Veenendaal, M., Devereaux, T. P., Hill, J. P. & van den Brink, J. Resonant inelastic x-ray scattering studies of elementary excitations. *Rev. Mod. Phys.* **83**, 705–767 (2011).
8. Zhou, K.-J. et al. I21: an advanced high-resolution resonant inelastic x-ray scattering beamline at Diamond Light Source. *J. Synchrotron Radiat.* **29**, 563–580 (2022).
9. Gorelov, E. et al. Nature of the Mott transition in Ca_2RuO_4 . *Phys. Rev. Lett.* **104**, 226401 (2010).
10. Han, Q. & Millis, A. Lattice energetics and correlation-driven metal-insulator transitions: the case of Ca_2RuO_4 . *Phys. Rev. Lett.* **121**, 067601 (2018).
11. Riccò, S. et al. In situ strain tuning of the metal-insulator-transition of Ca_2RuO_4 in angle-resolved photoemission experiments. *Nat. Commun.* **9**, 4535 (2018).
12. Zhang, J. et al. Nano-resolved current-induced insulator-metal transition in the mott insulator Ca_2RuO_4 . *Phys. Rev. X* **9**, 011032 (2019).
13. Nakatsuji, S. et al. Mechanism of hopping transport in disordered Mott insulators. *Phys. Rev. Lett.* **93**, 146401 (2004).
14. Das, L. et al. Spin-orbital excitations in Ca_2RuO_4 revealed by resonant inelastic X-ray scattering. *Phys. Rev. X* **8**, 011048 (2018).
15. Gretarsson, H. et al. Observation of spin-orbit excitations and Hund’s multiplets in Ca_2RuO_4 . *Phys. Rev. B* **100**, 045123 (2019).
16. Fatuzzo, C. G. et al. Spin-orbit-induced orbital excitations in Sr_2RuO_4 and Ca_2RuO_4 : a resonant inelastic x-ray scattering study. *Phys. Rev. B* **91**, 155104 (2015).
17. Jain, A. et al. Higgs mode and its decay in a two-dimensional antiferromagnet. *Nat. Phys.* **13**, 633–637 (2017).
18. Li, J. et al. Multiorbital charge-density wave excitations and concomitant phonon anomalies in $\text{Bi}_2\text{Sr}_2\text{LaCuO}_{6+\delta}$. *Proc. Natl. Acad. Sci. USA* **117**, 16219–16225 (2020).
19. von Arx, K. et al. Resonant inelastic x-ray scattering study of $\text{Ca}_3\text{Ru}_2\text{O}_7$. *Phys. Rev. B* **102**, 235104 (2020).
20. Lin, J. Q. et al. Strongly correlated charge density wave in $\text{La}_{2-x}\text{Sr}_x\text{CuO}_4$ evidenced by doping-dependent phonon anomaly. *Phys. Rev. Lett.* **124**, 207005 (2020).
21. Wang, Q. et al. Charge order lock-in by electron-phonon coupling in $\text{La}_{1.675}\text{Eu}_{0.2}\text{Sr}_{0.125}\text{CuO}_4$. *Sci. Adv.* **7**, <https://doi.org/10.1126/sciadv.abg7394> (2021).
22. Geondzhan, A. et al. Large polarons as key quasiparticles in SrTiO_3 and SrTiO_3 -based heterostructures. *Phys. Rev. Lett.* **125**, 126401 (2020).
23. Souliou, S.-M. et al. Raman scattering from higgs mode oscillations in the two-dimensional antiferromagnet Ca_2RuO_4 . *Phys. Rev. Lett.* **119**, 067201 (2017).
24. Vale, J. G. et al. High-resolution resonant inelastic x-ray scattering study of the electron-phonon coupling in honeycomb $a - \text{Li}_2\text{IrO}_3$. *Phys. Rev. B* **100**, 224303 (2019).
25. Dashwood, C. D. et al. Probing electron-phonon interactions away from the Fermi level with resonant inelastic x-ray scattering. *Phys. Rev. X* **11**, 041052 (2021).
26. Sutter, D. et al. Hallmarks of Hund’s coupling in the Mott insulator Ca_2RuO_4 . *Nat. Comm.* **8**, 15176 (2017).
27. Porter, D. G. et al. Magnetic anisotropy and orbital ordering in Ca_2RuO_4 . *Phys. Rev. B* **98**, 125142 (2018).
28. Forte, F., Cuoco, M. & Noce, C. Field-induced orbital patterns in ferromagnetic layered ruthenates. *Phys. Rev. B* **82**, 155104 (2010).
29. Kim, B. H. & van den Brink, J. Resonant inelastic x-ray scattering on single magnons at oxygen K edges. *Phys. Rev. B* **92**, 081105 (2015).
30. Fukazawa, H., Nakatsuji, S. & Maeno, Y. Intrinsic properties of the Mott insulator $\text{Ca}_2\text{RuO}_{4+\delta}$. *Phys. B* **281**, 613–614 (2000).
31. Nakatsuji, S. & Maeno, Y. Synthesis and single-crystal growth of $\text{Ca}_{2-x}\text{Sr}_x\text{RuO}_4$. *J. Solid State Chem.* **156**, 26 – 31 (2001).

Acknowledgements

We thank I. Bialo for insightful discussions. K.v.A. and J.C. acknowledge support by the Swiss National Science Foundation through Grant Number 200021-188564. K.v.A. is grateful for the support from the FAN Research Talent Development Fund—UZH Alumni and thanks the Forschungskredit of the University of Zurich, grant no. [FK-21-105]. Q.W. was supported by the Research Grants Council of Hong Kong (CUHK 24306223), and the CUHK Direct Grant (No. 4053613). Y.S. is supported through the Knut and Alice Wallenberg Foundation through the grant 2021.0150 and thanks the Chalmers Area of Advances-Materials Science and the Swedish Research Council (VR) with a starting Grant (Dnr. 2017-05078) for funding. F.F. and R.F. acknowledge support from the Italian Ministry of University and Research (MUR) under Grant PRIN No. 2020JZ5N9M (CONQUEST). F.F. acknowledges support from the National Recovery and Resilience Plan (NRRP), Call PRIN 2022, funded by the European Union—NextGenerationEU, Mission 4, Component 2, Grant No. 2022TWZ9NR (STIMO)-CUP B53D23004560006. M.C. acknowledges partial support from the EU Horizon 2020 research and innovation program under Grant Agreement No. 964398 (SUPERGATE) and, together with F.F., from NRRP MUR project PE0000023-NQSTI. This work was supported in part by the Italian Ministry of Foreign Affairs and International Cooperation, grant number KR23GR06. We acknowledge Diamond Light Source for time on Beamline I21 under proposal MM27638.

Author contributions

A.V. and R.F. grew the Ca_2RuO_4 single crystals. K.v.A., Q.W., J.Choi, M.G.-F., S.A., K.Z., Y.S., and J.Chang carried out the RIXS experiments. P.R. and K.v.A. analysed the data with support from Q.W., L.M., and J.Chang. F.F. developed the theoretical model and carried out the calculations with the help of M.C. K.v.A., F.F., M.C., and J.Chang wrote the manuscript with input from all authors.

Competing interests

The authors declare no competing interests.

Additional information

Supplementary information The online version contains supplementary material available at <https://doi.org/10.1038/s42005-025-02104-2>.

Correspondence and requests for materials should be addressed to Filomena Forte.

Peer review information *Communications Physics* thanks Jonathan Pellicciari and the other, anonymous, reviewer(s) for their contribution to the peer review of this work.

Reprints and permissions information is available at <http://www.nature.com/reprints>

Publisher’s note Springer Nature remains neutral with regard to jurisdictional claims in published maps and institutional affiliations.

Open Access This article is licensed under a Creative Commons Attribution 4.0 International License, which permits use, sharing, adaptation, distribution and reproduction in any medium or format, as long as you give appropriate credit to the original author(s) and the source, provide a link to the Creative Commons licence, and indicate if changes were made. The images or other third party material in this article are included in the article's Creative Commons licence, unless indicated otherwise in a credit line to the material. If material is not included in the article's Creative Commons licence and your intended use is not permitted by statutory regulation or exceeds the permitted use, you will need to obtain permission directly from the copyright holder. To view a copy of this licence, visit <http://creativecommons.org/licenses/by/4.0/>.

© The Author(s) 2025